Journal Name

ARTICLE

Structures and magnetic anisotropies of two seven-coordinate Co(II)-nitrate complexes showing slow magnetic relaxation

Received 00th January 20xx,
Accepted 00th January 20xx

DOI: 10.1039/x0xx00000x

www.rsc.org/

Wei Lv,[a] Lei Chen,[b] Xue-Tai Chen,*[a] Hong Yan,*[a] Zhenxing Wang,*[c] Zhong-Wen Ouyang,[c] and Zi-Ling Xue[d]

Two seven-coordinate Co(II)-nitrate complexes, $[Co(tmpdc)(NO_3)_2]$ (**1**) and $[Co(tmpdt)(NO_3)_2]\cdot CH_3CN$ (**2**) (tmpdc = N,N,N′,N′-tetramethyl-2,6-pyridinedicarboxamide, tmpdt = N,N,N′,N′-tetramethyl-2,6-pyridinedithiocarboxamide) with tridentate neutral ligands tmpdc or tmpdt have been prepared. Their crystal structures by single X-ray diffraction show markedly different coordination geometries when two donor atoms of the tridentate ligand change from oxygen in **1** to sulfur in **2**. Complex **1** is a capped octahedral while complex **2** is a pentagonal bipyramid. Results of direct-current (dc) magnetic measurements and high-frequency electron paramagnetic resonance (HFEPR) indicate the anisotropic S = 3/2 spin ground state of the Co(II) ions with the easy-plane anisotropy for both **1** and **2**. Frequency- and temperature-dependent alternating-current (ac) magnetic susceptibility studies reveal slow magnetic relaxation for **1** and **2** under applied fields.

Introduction

Over the last three decades, single-molecule magnets (SMMs)[1] have attracted increasing attention due to their interesting magnetic properties and potential applications in ultrahigh density memory components, quantum computation, spintronic devices and processing technologies.[2] Various types of SMMs, especially those based on the polynuclear clusters of the transition metal and/or lanthanide ions, have been extensively studied.[3,4] Recently, particular attention has been paid to SMMs containing single paramagnetic metal centre known as single-ion magnets (SIMs), as their magnetic properties can be easily finetuned via the variation of donor atoms and ligand fields. [4a, 5]

Since the first SIM based on an Fe(II) ion was found in 2010,[6] a great number of the SIMs with various first-row transition metals have been reported.[5,7] Among them, Co(II) SIMs have been found to be the largest family due to its strong magnetic anisotropy and the half-integer spin (S = 3/2). As a result, magnetic anisotropy and magnetic relaxation of Co(II)-SIMs with coordination numbers from two to eight have been reported.[7] Great effort is devoted to constructing SIMs with low coordination numbers, low oxidation states and high symmetry because of their strong magnetic anisotropy. [8-9] A record energy barrier of 450 cm^{-1} was found for a two-coordinate linear Co(II)-SIM, $Co(C(SiMe_2ONaph)_3)_2$ (Me = methyl, Naph = naphthyl group).[8a] However, low-coordinate SIMs are usually unstable and difficult to prepare. Thus more stable four-, five- and six-coordinate Co(II) complexes have been extensively studied and formed the vast majority of Co(II)-SIMs.[7] Co(II) complexes with high coordination numbers (7 or 8) also exhibit SIM behaviors.[10-18] To date, the majority of seven-coordinate Co(II)-SIMs adopt pentagonal bipyramid geometry.[10,11] In comparison, the seven-coordinate Co(II)-SIMs with other coordination geometries are relatively limited, as summarized in Table S1 (ESI). They have face-capped trigonal prism,[12-15] face-capped octahedral[16] or irregular geometry.[17] The only reported Co(II)-SIM with capped octahedral geometry contains a Co(II) centre restrained within a polydentate tripodal iminopyridine ligand.[16] Nearly all of the seven-coordinate Co(II)-SIMs exhibit easy-plane anisotropy with positive zero-field splitting D parameters, typically in the range of +20 and +45 cm^{-1},[10,11] except for $[(OTftpy)Co(NO_3)_2]$ (OTftpy = 4′-trifluoromethylsulfonate-2,2′:6′,2″-terpyridine) reported by Shores et al.[12] Its reported D value of -41.4 cm^{-1} was solely estimated by static magnetic data. It should be noted that this compound was described as a pentagonal bipyramid. Our CShM analysis with Shape 2.1 program shows that its coordination geometry is more likely a capped trigonal prismatic geometry since the deviation parameter relative to capped trigonal prismatic geometry (2.040) is smaller than that of pentagonal bipyramid (7.400) (Table S2, ESI).

It is well known that the single-ion magnetic anisotropy, the key factor for the performance of SIMs of transition metal ion with

[a] State Key Laboratory of Coordination Chemistry, School of Chemistry and Chemical Engineering, Nanjing University, Nanjing 210023, China. E-mail: xtchen@nju.edu.cn.
[b] School of Environmental and Chemical Engineering, Jiangsu University of Science and Technology, Zhenjiang 212003, P. R. China, E-mail: chenlei@just.edu.cn; aihua.yuan@just.edu.cn
[c] Wuhan National High Magnetic Field Center& School of Physics, Huazhong University of Science and Technology, Wuhan 430074, China
[d] Department of Chemistry, University of Tennessee, Knoxville, Tennessee 37996, USA.

†Electronic supplementary information (ESI) available: Table for the summary of the reported five-coordinate Co(II)-SIMs; Table for the calculations by SHAPE; Table for the fitting data for the Cole-Cole plot; Table for the theoretical calculation data; Figures of XRD patterns for **1-2**; Additional figures for magnetic characterization, HFEPR data and theoretical calculations; Additional structural data in CIF format (CIF). See DOI: 10.1039/x0xx00000x

a finite spin number, is affected by a few factors, including the nature of donors, ligand field and the intrinsic spin-coupling.[5,7] The type of donor atoms has been used to tune the magnetic anisotropy. Several studies have showed that heavier donor atoms like S, Se, Te, P and As give larger anisotropy in metal complexes.[19]

With the aims to study magnetic anisotropy of seven-coordinate Co(II) complexes, especially those with geometries other than pentagonal bipyramid, and the effect of donor atoms on the anisotropy, we have prepared two seven-coordinate Co(II) complexes bearing tridentate ligands, [Co(tmpdc)(NO_3)$_2$] (**1**) and [Co(tmpdt)(NO_3)$_2$]·CH_3CN (**2**) (tmpdc = N,N,N',N'-tetramethyl-2,6-pyridinedicarboxamide, tmpdt = N,N,N',N'-tetramethyl-2,6-pyridinedithiocarboxamide, Chart 1) with capped octahedral and distorted pentagonal bipyramid geometries, , respectively. Direct-current (dc) susceptibility data show that both **1** and **2** exhibit easy-plane magnetic anisotropy which has been confirmed by high frequency electron paramagnetic resonance (HFEPR) spectroscopy. Alternating-current (ac) magnetic susceptibility measurements demonstrated the field-induced slow magnetization relaxation in both complex **1** and **2**.

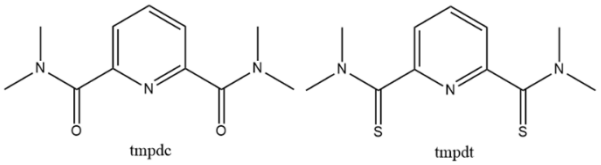

Chart 1

Experimental

Synthesis and general characterization

All solvents and other chemicals employed were commercially available and used without further purification except that acetonitrile used in the synthesis of **2** was purified by conventional methods before use. Elemental analyses were performed on an Elementar Vario ELIII elemental analyser. Powder X-ray diffraction (PXRD) patterns were recorded on a Bruker D8 ADVANCE X-ray powder diffractometer with a Cu Kα X-ray source (λ = 1.54056 Å) operated at 40 kV and 40 mA.

Synthesis of the ligands

The ligand tmpdc was prepared by published procedures,[20] while the ligand tmpdt was synthesized from tmpdc by a modified method.[21]

Synthesis of complexes 1 and 2

[Co(tmpdc)(NO_3)$_2$] (1). The method to prepare **1** has been reported previously.[22] $Co(NO_3)_2·6H_2O$ (0.73 g, 2.5 mmol) and tmpdc (0.55 g, 2.5 mmol) were dissolved in acetonitrile (50 mL). The mixture was stirred overnight and filtered. Red lamellate crystals were obtained from the diffusion of the diethyl ether into the solution in one week in 45% yield based on Co. Anal. Calc. for $C_{11}H_{15}CoN_5O_8$: C, 32.68; H, 3.75; N, 17.33. Found: C, 32.96; H, 3.82; N, 17.70.

[Co(tmpdt)(NO_3)$_2$]·CH_3CN (2). Complex **2** was prepared according to the modified procedure carried out under anhydrous conditions.[23] In a 100 mL Schlenk flask, anhydrous $CoCl_2$ (0.15 g, 1.19 mmol) and $AgNO_3$ (0.40 g, 2.38 mmol) were dissolved in anhydrous acetonitrile (20 mL) and stirred for 30 min. The white precipitate AgCl was removed by filtration and the pink filtrate was then added to the solution of tmpdt dissolved in anhydrous acetonitrile (20 mL). The mixture turned brown gradually and was kept stirring overnight. After filtration, the solution was put under the vapor of Et_2O and sealed to keep anhydrous in a cold environment (about 5 °C). Black block crystals were obtained after several weeks in a yield of 24% based on Co. Anal. Calc. for $C_{11}H_{15}CoN_5O_6S_2$: C, 30.28; H, 3.47; N, 16.05. Found: C, 31.178; H, 3.404; N, 15.277.

X-ray single-crystal structure determination

Single-crystal X-ray crystallographic data were collected for **1** and 2 by using a Bruker APEX DUO diffractometer at 296 K with a CCD area detector (Mo Kα radiation, λ = 0.71073 Å).[24] The APEXII program was used for collecting frames of data and determining the unit cell parameters. The data were integrated with SAINT program[25] and corrected for Lorentz factor and polarization effects. The absorption corrections were applied using SADABS.[26] The molecular structures were solved and completed via full-matrix least-squares procedure SHELXL (*Version 2018/3*).[27] The Co atom was determined first using the difference Fourier maps and then the other non-hydrogen atoms were subsequently identified. All non-hydrogen atoms were refined anisotropically and hydrogen atoms were set and generated as riding on the corresponding non-hydrogen atoms.

Magnetic measurements

Magnetic measurements were performed using a vibrating sample magnetometer (VSM) of Quantum Design MPMS SQUID-VSM system (1–1000 Hz) and a Physical Property Measurement System (PPMS) (10–10000 Hz). Variable-temperature dc susceptibility data of **1** and **2** were collected under a field of 0.10 T in the range of 2.0-300 K. The field-dependent magnetizations were measured in the range of 1-7 T at 1.9 K, 3.0 K and 5.0 K. The ac measurements were carried out with an oscillating ac field of 2 Oe under 0.2 T at 1.9 K and at frequencies from 1 to 1000 Hz to search for optimal magnetic field. After that, alternating-current (ac) susceptibility measurements of **1** and **2** were carried out on PPMS with an oscillating ac field of 2 Oe for **1** at 1.8 K under 0.15 T external field at frequencies ranging from 10 to 10000 Hz. All magnetic susceptibilities data were corrected for the diamagnetic contributions of the sample holder as well as for diamagnetism of the sample using Pascal's constants.[28]

HFEPR measurements.

HFEPR spectra were recorded on a locally developed spectrometer at the Wuhan National High Magnetic Field Center, China.[29-30] The microwaves of the transmission-type instrument are propagated by over-sized cylindrical light pipes. The samples were measured with KBr and pressed into pellets to minimize the effect of field-induced torquing.

Results and discussion

Structure Features

The crystal structure of **1** has been reported in the literature.[22] We re-determined its structure along with **2** for comparison. As illustrated in Table S3 (ESI), **1** crystalizes in the monoclinic space group $P2_1/n$ (No. 11) while **2** crystalizes in the triclinic space group $P\bar{1}$ (No. 2). The Co(II) ion in **1** is coordinated by one tridentate tmpdc ligand via O, N, O atoms and two bidentate nitrate anions (Fig. 1). In **2**, the Co(II) center is coordinated with S, N, S atoms of a tmpdt ligand and four O atoms from two nitrate anions. Moreover, two CH_3CN molecule is found in a unit cell of **2**.

Selected bond lengths and bond angles of **1** and **2** are listed in Table S4 (ESI). The Co-O bonds with the carboxamide group in **1** are 2.1757(1) and 2.1879(1) Å while the Co-S bonds in **2** is longer (2.4474(5) Å and 2.4380(5) Å). This difference is obviously due to the smaller atomic radius of O atom compared to the S atom, which also causes the shorter Co1-N2 bond length in **1** (2.0648(1) Å) than that in **2** (2.0979(1) Å). The lengths of Co-O bond involving nitrate groups are similar in the range of 2.1452(1)-2.2400(1) Å for **1** and 2.1294(1)-2.4768(1) Å for **2**, respectively. The nitrate groups coordinate to the Co(II) ion in unsymmetrical bidentate mode with a shorter and a longer Co-O bond. The most seriously unsymmetrical mode is found for one nitrate group in **2**, in which bond length of Co1-O1 (2.4768(1) Å) is >0.2 Å longer than the other Co-O bond (2.2688(1) Å). Similar coordination mode of nitrate anion has been reported in other seven-coordinate Co-nitrate complexes.[11a,17] The shortest intermolecular Co-Co distances are 8.289 Å for **1** and 6.154 Å for **2**.

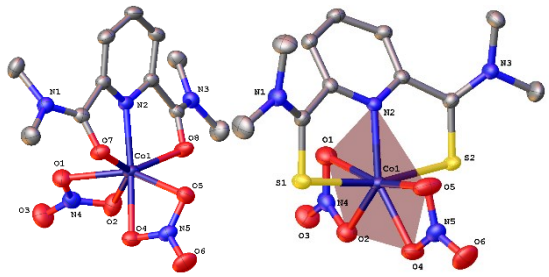

(a) (b)

Fig. 1 Structures of the anions in **1** and **2**. Blue, red, light blue, yellow and grey spheres represent Co, O, N, S and C atoms. Solvent molecules and H atoms are omitted for clarity.

The coordination geometry of complex **1** was previously described as distorted pentagonal bipyramid.[22] There are several coordination geometries for the seven-coordinate complexes. The continuous shape measure (CShM) is the most reliable method to determine the geometries especially for high-coordinate metal complexes.[31] CShM analysis with Shape 2.1 was performed for **1** to evaluate the degree of deviation in respect with the ideal seven-coordinate geometries (Table S5, ESI).[31] A large value of 8.075 was found relative to the ideal pentagonal bipyramid. In comparison, a value of 2.437 was found with respect to the capped octahedral geometry. Therefore, the coordination geometry of **1** can be described as capped octahedral rather than pentagonal bipyramid. Similar analysis of **2** showed that coordination geometry of **2** approaches a pentagonal bipyramid with the deviation value of 2.805. These observations indicated that the preferable coordination geometry varies when the O atom in tmpdc was replaced by S in tmpdt.

Close examination of the structural parameters might give some implications to the coordination geometrical variation. The Co-S bonds (2.4474(5) Å and 2.4380(5) Å) of tmpdt in **2** are much longer than Co-O bonds (2.1757(1) Å and 2.1879(1) Å) of tmpdc in **1**. These differences enable tmpdt to wrap around the Co centre in almost a semicircle shape supported by the larger angle of S1-Co1-S2 (166.427(1)°) compared with O1-Co1-O2 (139.56(5)°) in **1**. This semicircle coordination environment squeezes two nitrate anions away from the S1-Co1-S2 plane. The five atoms N2-O1-O2-O4-O5 atoms form a pentagonal plane approximately with the distance between Co atom and the plane centroid of 0.047 Å. Finally, the five atoms N2-O1-O2-O4-O5 atoms form an equatorial plane with the S1 and S2 atoms as the axial atoms which totally form a pentagonal bipyramid.

Intermolecular hydrogen bonds in complex **1** have been previously reported by Kapoor et al. in detail.[22] Similarly, hydrogen bonding exists in the crystal structure of **2**. For each molecule, the nitrate oxygen O3 is donor to C1-H1B···O3^{ii} (2.519 Å, ^{ii} = +x, +y, +z + 1) to give 1-D chains. These parallel chains are linked by C6-H6···O6^{iii} (2.695 Å, ^{iii} = +x, y – 1/2, +z) and C7-H7···O6^{iii} (2.644 Å, ^{iii} = +x, y – 1/2, +z) H-bonds, leading to a 2-D sheet structure parallel to the *bc* plane (Fig. S3). Two 2D-sheets form a double-decker structure (Fig. S4) via H-bonding C10-H10C···O6^{i} (2.544 Å, ^{i} = -x + 1/2, -y + 1/2, -z + 1/2). The double-decker finally form the 3D structure by H-bonding C2-H2A···O4^{iv} (2.713 Å, ^{iv} = -x, -y – 1/2, -z – 1/2), C11-H11B···O3^{v} (2.649 Å, ^{v} = x + 1/2, +y, +z), C5-H5···O1^{vi} (2.550 Å, ^{vi} = +x, +y, +z – 1/2) and C1-H1···O1^{vi} (2.665 Å, ^{vi} = +x, +y, +z – 1/2) (Fig. S5).

Static magnetic properties

Variable-temperature dc magnetic susceptibilities of **1** and **2** were measured on polycrystalline powders at a field of 0.10 T between 2.0 K and 300 K. The resulting susceptibility-temperature $\chi_M T$ versus T curves are shown in Fig. 2. Room-temperature $\chi_M T$ values are 2.45 and 2.35 cm^3 K mol^{-1} for **1** and **2**, respectively, consistent with the value for an S = 3/2 ion with g = 2.29 and 2.24 for **1** and **2**, respectively. These observed $\chi_M T$ products are much higher than the spin-only value of 1.875 cm^3 mol^{-1} K expected for an S = 3/2 system (g = 2.0), indicating a sizable contribution of orbital angular momentum. Similar trends can be observed in the $\chi_M T$-T plots of both **1** and **2**. Upon cooling, the $\chi_M T$ values decrease gradually to about 75 K, below which they decrease rapidly to the minimum values of 1.71 cm^3 K mol^{-1} and 1.31 cm^3 mol^{-1} K at 2 K, respectively. The sudden decline of the $\chi_M T$ value below 75 K is attributed to the presence of a strong magnetic anisotropy of Co(II) ions rather than the intermolecular interaction considering the long distance between the Co(II) ions.

Field-dependent magnetizations were measured under applied magnetic fields of 1-7 T at 1.9, 3.0 and 5.0 K (inset, Fig. 2). The magnetization values of 2.84 $N\mu_B$ and 2.00 $N\mu_B$ for **1** and **2** at 7 T and 1.9 K do not reach saturation. This non-saturation of magnetization at 7 T agrees with the presence of significant magnetic anisotropy.

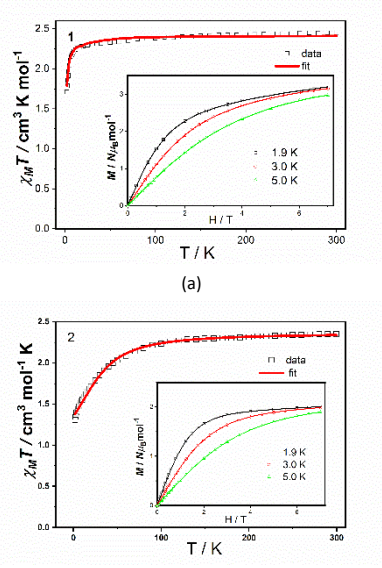

Fig. 2 Variable-temperature dc susceptibility data of **1** (a) and **2** (b) under 0.10 T applied dc field. Inset: field dependence of the magnetization below 5 K for **1** and **2**. Solid lines are the fits to the data with program *PHI*.[32]

To estimate the zero-field splitting (ZFS) parameters D and E values, both $\chi_M T$ versus T and M versus H curves were fit simultaneously with the following spin Hamiltonian (eqn. 1) employing the *PHI* program,[32]

$$H = D(\hat{S}_z^2 - S(S+1)/3) + E(\hat{S}_x^2 - \hat{S}_y^2) + \mu_B g\hat{S}\cdot H \quad (1)$$

where μ_B is the Bohr magneton, g is a tensor, S is the spin operator, H is the magnetic field vector, and D and E represent the axial and rhombic zero-field splitting parameters, respectively. In addition, the intermolecular exchange interactions with the zj parameter were considered. Reasonable fitting results could be obtained if the isotropic g value is employed in the fitting, which gave the parameters D = +4.73(3), E = 0.96(4), g = 2.23(6), zj = 0.01 cm^{-1} for **1** and D = +37.41(4), E = 11.42(2), g = 2.23(9), zj = -0.03 cm^{-1} for **2**. The positive sign of D value was further confirmed by the fact that the fitting could not give the reasonable agreement when D was set negative. It is known that the static magnetic data usually cannot yield the accurate values for D and E, especially their signs. Therefore, high-field EPR (HFEPR) studies were performed for **1** and **2**.

HFEPR studies

Polycrystalline samples of **1** and **2** were investigated by HFEPR spectroscopy using different frequencies and magnetic fields. There are several features observed in the spectrum of **1** in the frequency range from 60 to 420 GHz at 2 K. A typical spectrum at 154 GHz is shown in Fig. 3a. A 2D resonating field versus frequency curve of **1** was established from a series of the spectra at the different frequencies at 2 K and plotted in Fig. 3b where the EPR transitions are shown as squares. These experimental data show that not only intra-Kramers transitions within the lowest doublet $M_S = \pm 1/2$ with $\Delta M_S = \pm 1$ but also inter-Kramers transitions between $M_S = \pm 1/2$ and $M_S = \pm 3/2$ Kramers doublets have been observed in spectra. All the experimental points can be simultaneously fit by spin Hamiltonian (eqn. 1) using the program SPIN[33] to give the optimal parameters: $|D|$ = 3.65 cm^{-1}, E = 0.70 cm^{-1}, $g_x = g_y$ = 2.33, and g_z = 2.25. In order to reveal the sign of D value, the EPR spectrum recorded at 154 GHz and 2 K was also simulated using the above Hamiltonian parameters. Comparing the experimental spectrum to the simulated ones obtained with both positive and negative D values shows that the sign of D value was positive rather than negative (Fig. 3a).

Three features are observed in the HFEPR spectra for **2** at the frequency range from 60 to 420 GHz at 2 K. A typical spectrum at 60 GHz is shown in Fig. 4a. The 2D resonance fields versus frequency curve of **2** was plotted in Fig. 4b, where the experimental points are all located in three three straight lines. Such transition patterns indicate that only intra-Kramers transitions within the lowest doublet $M_S = \pm 1/2$ with $\Delta M_S = \pm 1$ are observed in spectrum. Given the magnitude of D from the fitting of the dc magnetic data (D = 37.41 cm^{-1}), the simulations were conducted by the spin-Hamiltonian (eqn. 1) with SPIN program[34] assuming an axial g-tensor ($g_x = g_y$), yielding the parameters D = +37.41 cm^{-1}, E = 6.82 cm^{-1}, $g_x = g_y$ = 2.32, g_z = 2.16. The positive sign was confirmed by the comparison of the experimental spectrum at 60 GHz with the simulation ones of positive and negative sign of the D values (Fig. 4a).

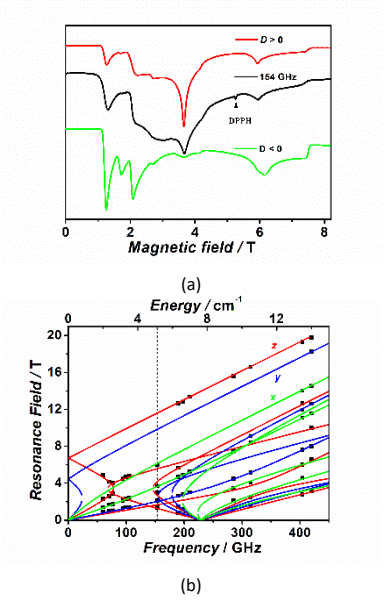

Fig. 3 (a) Typical HFEPR spectrum of **1** at 154 GHz and 2 K (black) with the simulations using spin Hamiltonian with the true spin S = 3/2 (red: D > 0; green: D < 0). (b) Resonance field vs. macrowave frequency for EPR transitions for **1** at 2 K. The squares are the experimental points while green, blue and red curves are generated by fitting using program SPIN[33] with the magnetic field parallel to the x, y and z axes of the ZFS tensors, respectively.

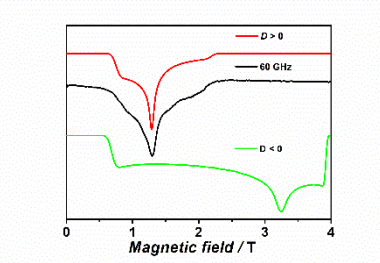

(a)

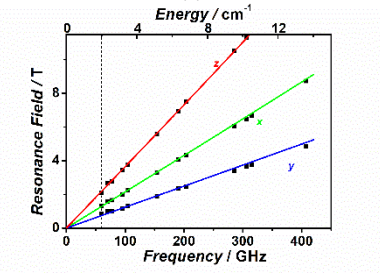

(b)

Fig. 4 (a) Typical HFEPR spectrum of **2** at 60 GHz and 2 K (black) with the simulations using spin Hamiltonian with the true spin S = 3/2 (red: D > 0; green: D < 0). (b) Resonance field vs. macrowave frequency for EPR transitions for **2** at 2 K. The squares are the experimental points while green, blue and red curves are generated by fitting using program SPIN[33] with the magnetic field parallel to the x, y and z axes of the ZFS tensors, respectively.

Dynamic magnetic properties

In order to study the single molecular magnetism for **1** and **2**, temperature- and frequency-dependent alternating-current (ac) susceptibilities were studied on polycrystalline samples of **1** and **2**. The field-dependent measurements were performed with an alternating field of 0.2 mT oscillating with 1–1000 Hz under different dc fields up to 0.3 T at 1.8 K for **1** and **2**, respectively (Fig. S8, ESI). No out-of-phase ac susceptibility signals (χ''_M) are observed under zero-field probably due to the occurrence of quantum tunneling of the magnetization (QTM). The application of applied magnetic field could suppress the QTM effect and induce the significant frequency-dependent χ''_M signals. The data indicates the optimum field to reduce the QTM effect for **2** is 0.1 T. But for **1**, there are no χ''_M signal peaks observed in the field-dependent measurements (Fig. S8a), implying that the observation of complete relaxation process requires a wider frequency range. Subsequently, ac susceptibility measurements up to 10000 Hz under the different applied static fields from 0 to 0.3 T were conducted on **1** (Fig. S9). The best applied ac measurement field for complex **1** is 0.15 T. These results prove that both **1** and **2** are field-induced SIMs.

Further ac measurements were conducted in the range of 1.8-3.6 K under 0.15 T for **1** and 1.8-3.8 K under 0.1 T for **2** (Fig. 5). The peak of χ_M'' signal appears at 446.7 Hz at 1.8 K under 0.15 T for **1** and 31.6 Hz at 1.8 K under 0.1 T for **2**. With the temperature increasing, the peak value of χ''_M signals shift gradually to higher frequency region.

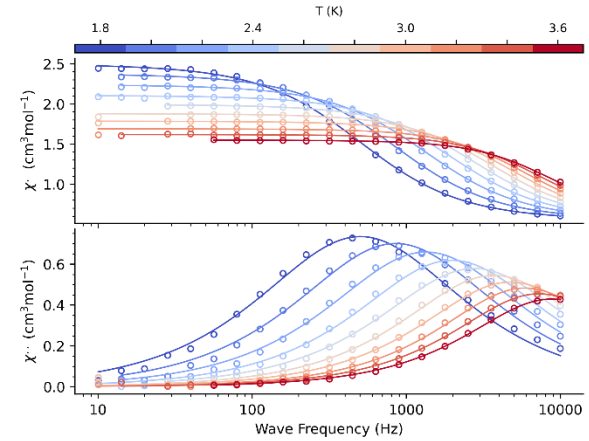

(a)

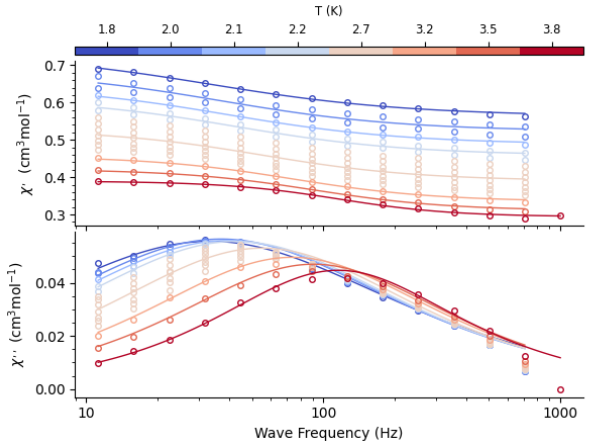

(b)

Fig. 5 Frequency dependence of the ac susceptibility from 1.8 K to 3.6 K for **1** (a) at 0.15 T and from 1.8 K to 3.8 K for **2** (b) at 0.2 T, respectively. The solid lines are for eye guide.

As is shown in Fig. 6, the Cole–Cole plots of **1** and **2** were generated from the ac susceptibility data and fitted via the generalized Debye model[34-35] by CCFIT2 program[36] (eqn. 2) to extract the values and distribution of the relaxation times.

$$\chi_{ac}(\omega) = \chi_S + \frac{\chi_T - \chi_S}{1 + (i\omega\tau)^{(1-\alpha)}} \qquad (2)$$

where χ_T and χ_S are the isothermal and the adiabatic susceptibility, respectively; ω is angular frequency; τ is the relaxation time; α indicates the deviation from a pure Debye model. The fitting parameters are summarized in Table S6. The obtained α values are in the range of 0.0721(6)-0.178(8) for **1** under 0.15 T and in the range of0.04(3)–0.28(2) for **2** under 0.1 T (Table S6), indicating the relatively narrow distribution of the relaxation times.

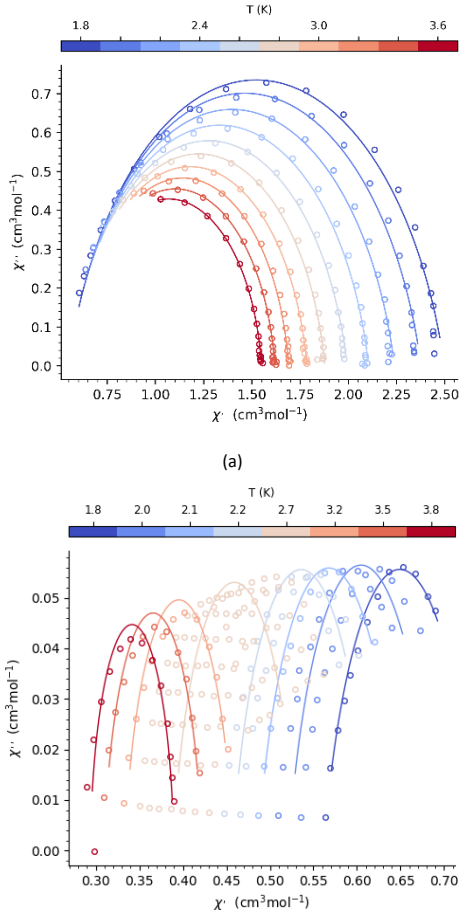

Fig. 6 Cole-Cole plots for **1** under 0.15 T (a) and for **2** under 0.1 T (b) dc field. The solid lines are the best fits to the experiments with the generalized Debye model.

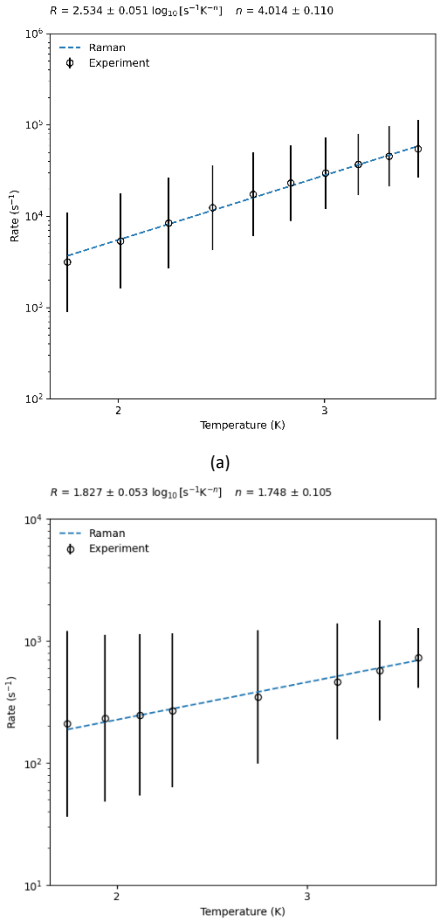

Fig. 7 The plots of relaxation Rates versus T for **1** under 0.15 T (a) and for **2** under 0.1 T (b).

The origin of the slow relaxation of magnetization in Kramers ions with dominant easy-plane magnetic anisotropy has been investigated in detail.[37] Such spin-lattice relaxation can be described by one-phonon direct processes and/or two-phonon Raman processes. The temperature dependence of the relaxation times was successfully fitted considering the Raman relaxation mechanism described by equ 3,

$$\tau^{-1} = CT^n \quad (3)$$

The fitting results by CCFIT2 program[36] gave C = 392(1) s^{-1}, n = 4.0(1) for **1** and C = 67(1) s^{-1}, n = 1.7(1) for **2** (Fig. 7). The fittings including the Orbach and/or direct process could not give reasonable results.

The above fittings for **1** and **2** show that the simulated data are in good agreement with the experimental ones, but the n values for both **1** and **2** are much less than 9 previoulsy expected for the Raman process of a Kramers ion.[39a] Similar small values of n have been reported for other Co(II)-SIMs.[11a,11d,11e,38] Recent research suggest that n = 1-6 can also occur for Raman process, which is due to modulating magnetic interactions by intramolecular vibrations.[39]

Conclusions

Two seven-coordinate Co(II)-nitrate complexes were prepared by the treatment of $Co(NO_3)_2.6H_2O$ with tmpdc and tmpdt. Single crystal X-ray crystallographic studies of **1** and **2** show that the variation of two donor atoms play a significant role in the molecular structures of **1** and **2**. Even though the coordination mode of the tridentate ligand and the nitrate anion are similar in these two complexes, their coordination geometries are different. The coordination geometry of **1** is close to a capped octahedral geometry while complex **2** has a pentagonal bipyramid geometry.

The static magnetic properties of **1** and **2** have been investigated by dc magnetic measurements and HFEPR. The results show the easy-plane anisotropy for **1** and **2** but the zero-field splitting parameter D for **1** is much smaller than **2**, which could be due to the markedly different coordination geometry and the nature of donor atom.

Both complexes have been found to be field-induced single-ion magnets, showing the frequency-dependent out-of-phase ac susceptibility signals. The magnetic relaxation of **1** is faster than **2**. The relaxation times at different temperatures

can be fitted by a power law, indicating that the Raman mechanism is the dominant process in the magnetic relaxation of **1** and **2** below 4.0 K and the relaxation over 4 K for **2** is mainly dominated by Orbach Process. Complex **1** represents a new example of seven-coordinate Co(II)-SIM with a geometry close to a capped octahedron.

Due to the unclear relationship between coordination geometry and magnetic properties in the seven-coordinate Co(II) complexes, much more work on those complexes with coordintion geometry other than pentagonal bipyramid will be necessary in the future.

Conflicts of interest

There are no conflicts to declare.

Author contributions

Wei Lv: synthesis, characterization, structural determination and manuscript writing; Lei Chen: magnetic and EPR modelling; Zhenxing Wang, Zhong-Wen Ouyang: HFEPR measurements and interpretations; Xue-Tai Chen, Hong Yan, Zi-Ling Xue: project design and writing.

Acknowledgments

We are grateful for the financial support from the Natural Science Grant of China (No. 21471078 to XTC), the National Key Research and Development Program of China (2021YFA1600304 to ZXW) and the Joint Fund for Regional Innovation and Development (U20A2073 to ZXW).

Notes and references

1 (a) D. Gatteschi, R. Sessoli and J. Villain, *Molecular Nanomagnets*; Oxford University Press: Oxford, **2006**. (b) R. Winpenny, Ed. *Single-Molecule Magnets and Related Phenomena*; Springer: New York, **2006**

2 (a) W. Wernsdorfer and R. Sessoli, *Science*, 2009, **284**, 133-135. (b) M. N. Leuenberger and D. Loss, *Nature*, 2001, **410**, 789-793. (c) M. Affronte, *J. Mater. Chem.*, 2009, **19**, 1731-1737.

3 (a) R. Bagai and G. Christou, *Chem. Soc. Rev.*, 2009, **38**, 1011-1026. (b) K. S. Pedersen, J. Bendix and R. Clerac, *Chem. Commun.*, 2014, **50**, 4396-4415.

4 (a) D. N. Woodruff, R. E. P. Winpenny and R. A. Layfield, *Chem. Rev.*, 2013, **113**, 5110−5148. (b) A. Dey, J. Acharya and V. Chandrasekhar, *Chem. Asian J.*, 2019, **14**, 4433-4453.

5 (a) J. M. Frost, K. L. M. Harriman and M. Murugesu, *Chem. Sci.*, 2016, **7**, 2470−2491. (b) G. A. Craig and M. Murrie, *Chem. Soc. Rev.*, 2015, **44**, 2135−2147. (c) A. K. Bar, C. Pichon and J.-P. Sutter, *Coord. Chem. Rev.*, 2016, **308**, 346−380. (d) A. Sarkar, S. Dey and G. Rajaraman, *Chem.Eur. J.*, 2020, **26**, 14036-14058. (e) M. Feng and M. L. Tong, *Chem. Eur. J.*, 2018, **24**, 7574-7594.

6 D. E. Freedman, W. H. Harman, T. D. Harris, G. J. Long, C. J. Chang and J. R. Long, *J. Am. Chem. Soc.*, 2010, **132**, 1224-1225.

7 (a) R. S. Narayanan and V. Chandrasekhar, *Top. Organomet. Chem.*, 2019, **64**, 35–76. (b) P. K. Sahu, R. Kharel, S. Shome, S. Goswami, S. Konar, *Coord. Chem. Rev.*, 2023, **475**, 214871(1-22)

8 (a) P. C. Bunting, M. Atanasov, E. Damgaard-Moller, M. Perfetti, I. Crassee, M. Orlita, J. Overgaard, J. van Slageren, F. Neese and J. R. Long, *Science*, 2018, **362**, eaat7319. (b) X. N. Yao, J. Z. Du, Y. Q. Zhang, X. B. Leng, M. W. Yang, S. D. Jiang, Z. X. Wang, Z. W. Ouyang, L. Deng, B. W. Wang and S. Gao, *J. Am. Chem. Soc.*, 2017, **139**, 373−380.

9 (a) Y.-F. Deng, Z. Wang, Z.-W. Ouyang, B. Yin, Z. Zheng and Y.-Z. Zheng, *Chem. Eur. J.*, 2016, **22**, 14821–14825. (b) A. Eichhöfer, Y. Lan, V. Mereacre, T. Bodenstein and F. Weigend, *Inorg. Chem.*, 2014, **53**, 1962-1974. (c) F. Deng, T.Han, B. Yin and Y.-.Zheng, *Inorg. Chem. Front*., 2017, **4**, 1141–1148. (d) C. Das, A. Rasamsetty, S. Tripathi and M. Shanmugam, *Chem. Commun.*, 2020, **56**, 13397—13400.

10 J.-P. Sutter, V. Béreau, V. Jubault, K. Bretosh, C. Pichon and C. Duhayon, *Chem. Soc. Rev.*, 2022, **51**, 3280-3313.

11 (a) L. Chen, S. Y. Chen, Y. C. Sun, Y. M. Guo, L. Yu, X. T. Chen, Z. Wang, Z. W. Ouyang, Y. Song and Z. L. Xue, *Dalton. Trans.*, 2015, **44**, 11482-11490. (b) P. Antal, B. Drahos, R. Herchel and Z. Travnicek, *Inorg. Chem.*, 2016, **55**, 5957-5972. (c) M. A. Hay, C. J. McMonagle, C. Wilson, M. R. Probert and M. Murrie, *Inorg. Chem.*, 2019, **58**, 9691-9697. (d) A. K. Mondal, A. Mondal, B. Dey and S. Konar, *Inorg. Chem.*, 2018, **57**, 9999-10008. (e) M. Peng, X. F. Wu, L. X. Wang, S. H. Chen, J. Xiang, X. X. Jin, S. M. Yiu, B. W. Wang, S. Gao and T. C. Lau, *Dalton Trans.*, 2021, **50**, 15327-15335.

12 R. F. Higgins, B. N. Livesay, T. J. Ozumerzifon, J. P. Joyce, A. K. Rappé, M. P. Shores, *Polyhedron*, 2018, **143**, 193–200.

13 X. C. Huang, R. Xu, Y. Z. Chen, Y. Q. Zhang and D. Shao, *Chem. Asian J.*, 2020, **15**, 279-286.

14 G. Yi, H. Cui, C. Zhang, W. Zhao, L. Chen, Y. Q. Zhang, X. T. Chen, Y. Song and A. Yuan, *Dalton Trans.*, 2020, **49**, 2063-2067.

15 G. Yi, C. Zhang, W. Zhao, H. Cui, L. Chen, Z. Wang, X. T. Chen, A. Yuan, Y. Z. Liu and Z. W. Ouyang, *Dalton Trans.*, 2020, **49**, 7620-7627.

16 C. M. Klug, T. J. Ozumerzifon, I. Bhowmick, B. N. Livesay, A. K. Rappe and M. P. Shores, *Dalton Trans.*, 2019, **48**, 9117-9126.

17 L. Chen, H. H. Cui, S. E. Stavretis, S. C. Hunter, Y. Q. Zhang, X. T. Chen, Y. C. Sun, Z. Wang, Y. Song, A. A. Podlesnyak, Z. W. Ouyang and Z. L. Xue, *Inorg. Chem.*, 2016, **55**, 12603-12617.

18 (a) L. Chen, J. Wang, J. M. Wei, W. Wernsdorfer, X. T. Chen, Y. Q. Zhang, Y. Song and Z. L. Xue, *J. Am. Chem. Soc.*, 2014, **136**, 12213-12216. (b) X. X. Jin, X. X. Chen, J. Xiang, Y. Z. Chen, L. H. Jia, B. W. Wang, S. C. Cheng, X. Zhou, C. F. Leung and S. Gao, *Inorg. Chem.*, 2018, **57**, 3761-3774. (c) S. E. Stavretis, D. H. Moseley, F. Fei, H. H. Cui, Y. Cheng, A. A. Podlesnyak, X. Wang, L. L. Daemen, C. M. Hoffmann, M. Ozerov, Z. Lu, K. Thirunavukkuarasu, D. Smirnov, T. Chang, Y. S. Chen, A. J. Ramirez-Cuesta, X. T. Chen and Z. B. Xue, *Chem. Eur. J.*, 2019, **25**, 15846-15857.

19 (a) J. M. Zadrozny, J. Telser and J. R. Long, *Polyhedron*, 2013, **64**, 209−217. (b) F. Shao, B. Cahier, E. Riviere, R. Guillot, N. Guihery, V. E. Campbell and T. Mallah, *Inorg. Chem.*, 2017, **56**, 1104−1111. (c) X.-N. Yao, M.-W. Yang, J. Xiong, J.-J. Liu, C. Gao, Y.-S. Meng, S.-D. Jiang, B.-W. Wang and S. Gao, *Inorg. Chem. Front.*, 2017, **4**, 701−705. (d) M. R. Saber and K. R. Dunbar, *Chem. Commun.,* 2014, **50**, 12266−12269.

20 I. Okamoto, M. Terashima, H. Masu, M. Nabeta, K. Ono, N. Morita, K. Katagiri, I. Azumaya and O. Tamura, *Tetrahedron*, 2011, **67**, 8536-8543.

21 R. Kapoor, A. Kataria, P. Venugopalan, P. Kapoor, M. Corbella, M. Rodriguez, M. Romero and A. L. M. Sola, *Inorg. Chem.*, 2004, **43**, 6699-6706.

22 P. Kapoor, A. P. S. Pannu, M. Sharma, G. Hundal, R. Kapoor and M. S. Hundal, *J. Coord. Chem.*, 2011, **64**, 256-271.

23 R. Kapoor, A. Kataria, P. Kapoor and P. Venugopalan, *Transition Met. Chem.*, 2004, **29**, 425-429.
24 *SMART & SAINT Software Reference Manuals, version 6.45*, 2003Bruker Analytical X-ray Systems, Inc.: Madison, WI.
25 SAINT, *Siemens Analytical X-ray Instruments, Madison, WI*, 1994 - 1996.
26 G. M. Sheldrick, *SADABS: Software for Empirical Absorption Correction, version 2.05*, 2002, University of Göttingen: Göttingen, Germany.
27 G. M. Sheldrick, *Acta Crystallogr. Sect. C: Struct. Chem.*, 2015, **71**, 3-8.
28 G. A. Brain and J. F. Berry, *J. Chem. Educ.*, 2008, **85**, 532-536.
29 S. L. Wang, L. Li, Z. W. Ouyang, Z. C. Xia, N. M. Xia, T. Peng and K. B. Zhang, *Acta Phys. Sin*, 2012, **61**, 107601.
30 H. Nojiri and Z. W. Ouyang, *Terahertz Sci. Technol.*, 2012, **5**, 1-10.
31 (a) S. Alvarez, P. Alemany, D. Casanova, J. Cirera, M. Llunell and D. Avnir, *Coord. Chem. Rev.*, 2005, **249**, 1693-1708. (b) D. Casanova, P. Alemany, J. M. Bofill and S. Alvarez, *Chem. Eur. J.*, 2003, **9**, 1281-1295.
32 N. F. Chilton, R. P. Anderson, L. D. Turner, A. Soncini and K. S. Murray, *J. Comput. Chem.*, 2013, **34**, 1164-1175.
33 Simulations were performed using SPIN developed by Andrew Ozarowski of the National High Magnetic Field Laboratory, USA.
34 K. S. Cole and R. H. Cole, *J. Chem. Phys.*, 1941, **9**, 341-351.
35 Y. N. Guo, G. F. Xu, Y. Guo and J. Tang, *Dalton Trans.*, 2011, **40**, 9953-9963.
36 D. Reta and N. F. Chilton., *Phys. Chem. Chem. Phys.*, 2019, **21**, 23567-23575.
37 S. Gomez-Coca, A. Urtizberea, E. Cremades, P. J. Alonso, A. Camon, E. Ruiz and F. Luis, *Nat. Commun*, 2014, **5**, 4300(1-8).
38 (a) B. Drahos, R. Herchel and Z. Travnicek, *Inorg. Chem.*, 2017, **56**, 5076-5088. (b) A. Mondal, A. K. Kharwar and S. Konar, *Inorg. Chem.*, 2019, **58**, 10686-10693.
39 (a) A. Singh, K. N. Shrivastava, *Phys. Stat. Sol. B*, 1979, **95**, 273-277. (b) A. Lunghi, S. Sanvito, *J. Phys. Chem. Lett.,* 2020, **11**, 6273–6278. (c) M. Briganti, F. Santanni, L. Tesi, F. Totti, R. Sessoli, and A. Lunghi, *J. Am. Chem. Soc.*, 2021, **143**, 13633–13645.

